Extreme runoff generation from atmospheric river driven snowmelt during the 2017 Oroville Dam spillways incident

Brian Henn[1], Keith Musselman[2], Leanne Lestak[3], Marty Ralph[4], and Noah P. Molotch[3]

[1]Scripps Institution of Oceanography, UC San Diego
[2]Institute of Arctic and Alpine Research
[3]University of Colorado Boulder
[4]SIO

November 22, 2022

Abstract

In Feb. 2017, a five-day sequence of atmospheric river storms in California, USA, resulted in extreme inflows to Lake Oroville, the state's second-largest reservoir. Damage to the reservoir's spillway infrastructure necessitated evacuation of 188,000 people; subsequent infrastructure repairs cost $1 billion. We assess the atmospheric conditions, snowmelt, and runoff against major historical events. The event generated exceptional runoff volumes (second-largest in a 30 year record) partially at odds with the event precipitation totals (ninth-largest). We explain the discrepancy with observed record melt of deep antecedent snowpack, heavy rainfall extending to unusually high elevations, and high water vapor transport during the atmospheric river storms. An analysis of distributed snow water equivalent indicates that snowmelt increased water available for runoff watershed-wide by 37% (25-52% at 90% confidence). The results highlight an acute flood risk to public safety and infrastructure projected to increase in severity in a warmer and more variable climate.

Hosted file

`henn et al. 2020 - oroville snowmelt - supplement.docx` available at https://authorea.com/users/534330/articles/598455-extreme-runoff-generation-from-atmospheric-river-driven-snowmelt-during-the-2017-oroville-dam-spillways-incident

Extreme runoff generation from atmospheric river driven snowmelt during the 2017 Oroville Dam spillways incident

Brian Henn[1], Keith N. Musselman[2], and Leanne Lestak[2], F. Martin Ralph[1], and Noah P. Molotch[2,3]

[1]Center for Western Weather and Water Extremes, University of California San Diego, La Jolla, CA, USA

[2]Institute of Arctic and Alpine Research, University of Colorado Boulder, Boulder, CO, USA

[3]Jet Propulsion Laboratory, California Institute of Technology, Pasadena, CA, USA

Revised submission to *Geophysical Research Letters*

Corresponding author:

Brian Henn, bhenn@ucsd.edu, 9500 Gilman Drive #0224, La Jolla, CA 92093, USA

Key Points

- The atmospheric river event causing the 2017 Oroville Dam spillways incident was more exceptional for runoff than precipitation totals

- High rain-snow elevations, deep antecedent snowpack, and unprecedented snowmelt are shown to explain the discrepancy

- We highlight the importance of considering snowmelt, rain-snow elevations, and climate change in assessing current and future flood risk

Plain Language Summary

In Feb. 2017, extreme runoff into California's second-largest reservoir, Lake Oroville, and cracks in the reservoir's spillways resulted in evacuations of thousands of people and major repair costs. We analyzed to what extent the atmospheric river storms that caused the extreme runoff were unusual in terms of precipitation, snowmelt, temperature, and moisture in the air. We found that the precipitation amounts were much less unusual than the runoff amounts, suggesting that other factors were involved. We also found that snowmelt in the Sierra Nevada mountains above the reservoir was the heaviest on record at many locations, driven by unusually warm temperatures and deep pre-existing snowpack before the storms began. Thus, the warm temperatures and record melt likely increased the extreme runoff by about a third during the spillways incident. Our findings are consistent with other studies that suggest that unusually warm temperatures during winter atmospheric river storms in the Western United States are associated with flood risk due to substantial rainfall and snowmelt. Climate change is expected to increase the type of flood risk experienced in the 2017 Oroville Dam spillways incident.

Abstract

In Feb. 2017, a five-day sequence of atmospheric river storms in California, USA, resulted in extreme inflows to Lake Oroville, the state’s second-largest reservoir. Damage to the reservoir’s spillway infrastructure necessitated evacuation of 188,000 people; subsequent infrastructure repairs cost $1 billion. We assess the atmospheric conditions, snowmelt, and runoff against major historical events. The event generated exceptional runoff volumes (second-largest in a 30 year record) partially at odds with the event precipitation totals (ninth-largest). We explain the discrepancy with observed record melt of deep antecedent snowpack, heavy rainfall extending to unusually high elevations, and high water vapor transport during the atmospheric river storms. An analysis of distributed snow water equivalent indicates that snowmelt increased water available for runoff watershed-wide by 37% (25-52% at 90% confidence). The results highlight an acute flood risk to public safety and infrastructure projected to increase in severity in a warmer and more variable climate.

1. Introduction

In Feb. 2017, a sequence of atmospheric river (AR) storms made landfall in Northern California. The storms coincided with spillways failures at California's 2nd-largest reservoir, Lake Oroville (capacity 3.553 million acre-feet or 4.2 billion m^3) and resulted in the evacuation of 188,000 downstream residents (France et al., 2018; Vano et al., 2019). The situation was controlled without catastrophic flooding, but repair costs approached $1 billion and public disruption resulted from evacuations. While spillway failures (France et al., 2018) and atmospheric conditions (White et al., 2019) have been investigated, an unanswered question is the role of snowmelt in the event's exceptional runoff magnitudes.

In the Feb. 2017 AR sequence, the 10,200 km^2 Lake Oroville watershed in the northern Sierra Nevada experienced prolonged, heavy precipitation and high rain-snow elevations (Z_{RS}, height in the atmosphere at which snow melts into rain) on extensive and deep antecedent snowpack. ARs are the primary drivers of extreme precipitation in the U.S. West Coast (Ralph & Dettinger, 2012) and Sierra Nevada (Ralph et al., 2016), and have been shown to induce rain-on-snow flooding when warm, subtropical moisture increases rainfall rates and Z_{RS} (Guan et al., 2016; Lundquist et al., 2008; Wayand et al., 2015). Air temperature, humidity and wind speed conditions typical of ARs can generate substantial snowmelt due to latent heat release when moisture condenses on the snow surface (Marks et al., 1998). Z_{RS} is a critical component of landfalling ARs; its intersection with topography determines fractions of precipitation falling as rain and snow (Henn et al., 2020). Greater volatility in precipitation, temperature and snowmelt are expected with a warming climate (Musselman et al., 2018; Musselman et al., 2017; Swain et al., 2018), and so the Oroville Dam case may be a harbinger of climate-driven infrastructure risks.

White et al. (2019) examined precipitation, rain-snow elevations, and Lake Oroville inflows during the Feb. 2017 AR sequence. We assess its magnitude in a historical context using Generalized Extreme Value (GEV) return periods for atmospheric moisture flux, precipitation, temperature, snowmelt, and inflows. We estimate the extent to which melt of antecedent snowpack – driven by warm AR conditions and Z_{RS} – increased the terrestrial water input (TWI, rain plus snowmelt). To evaluate the role of snowmelt in runoff generation across the watershed, we use a distributed snow water equivalent (SWE) product from satellite and *in situ* observations.

2. Data and Methods

2.1 Precipitation and runoff

Precipitation observations for the Lake Oroville watershed were obtained from the California Nevada River Forecast Center (CNRFC; cnrfc.noaa.gov). The 6-hourly, 4 km resolution grids use gauge observations and topographic correction (Lin & Mitchell, 2005). We divided precipitation among each 6 hr period using relative accumulations in the hourly NLDAS-2 precipitation product (Xia et al. 2012; see S1). For a 1981-2017 precipitation climatology, we use Parameter Regression on Independent Slopes Model (PRISM, Daly et al., 1994) 4 km daily grids (available at prism.nacse.org). Inflows to Lake Oroville were estimated by the California Department of Water Resources (CDWR), using hourly mass balance from measured outflows from the powerhouse and spillways and reservoir storage observations (1988-present; cdec.water.ca.gov).

2.2 Radar rain-snow heights

We use hourly radar observations of the radar brightband height (Z_{BB}, a high-reflectivity feature that results from melting hydrometeors; White et al. 2002) made at a profiling radar at Oroville Dam (Figure 1a; White et al., 2013).

2.3 Atmospheric reanalysis

We use NASA's MERRA-2 reanalysis (Gelaro et al., 2017), available for years since 1981 and used elsewhere to diagnose and evaluate historical ARs (Jackson et al., 2016). Winds and moisture content over the atmospheric column were used to calculate integrated vapor transport (IVT; Ralph et al., 2004, 2005, 2019), interpolated from the ~0.5° MERRA-2 grid to Oroville Dam to produce a 3-hourly time series. 1981-2017 IVT climatology based on the MERRA-2 reanalysis was extracted following the methods of Rutz et al. (2014). We extract the height of the 0°C isotherm ($Z_{0°C}$) from MERRA-2 at the Oroville Dam location.

2.4 In situ snow water equivalent and snow depth

Daily SWE measurements were obtained from 12 weighing snow pillows (squares, Figure 1a), with records varying from 32 to 47 yr. Snowmelt was estimated as the daily SWE declines summed over an event period. We also examine SWE on about 1 Feb. 2017 at a network of manual snow survey courses (triangles, Figure 1a). Nearly all snow measurement sites are above the median watershed elevation (1,550 m); 80% of the watershed area has an elevation between 900 and 1,900 m (Figure 1b). To help infer precipitation phase (see S2), we use seven snow depth sensors (circles, Figure 1a), from networks maintained by CDWR and the University of California (Avanzi et al., 2018).

2.5 Distributed SWE product

To calculate watershed-wide changes in SWE, we use an interpolation approach that combines in situ snow pillow SWE measurements, MODIS satellite snow-cover observations, and historical patterns of reconstructed SWE (Schneider and Molotch 2016; see S4). We use 500 m resolution SWE maps from 24 Jan. 2017 and 12 Feb. 2017 (cloud-free satellite image dates nearest the AR sequence).

2.6 Partitioning of precipitation phase

To estimate the rain fraction, we partitioned the CNRFC precipitation into rain and snow using Z_{RS}. We estimate Z_{RS} from radar Z_{BB} at Oroville Dam and MERRA-2 $Z_{0°C}$. Z_{BB} is a direct observation of Z_{RS} above the watershed, but it is not observed at all hours. Therefore, we predict Z_{RS} using a model with MERRA-2 $Z_{0°C}$:

$$Z_{RS} = \beta_0 + \beta_1 Z_{0°C} + \varepsilon \sim N(0, \sigma^2) \quad (1)$$

where $\boldsymbol{\beta}$ and σ are model coefficients fitted to 101 corresponding MERRA-2 and radar brightband values over winter 2016-2017. We find that β_0 is -296 m, β_1 is 0.97, and σ is 215 m, with model R^2 of 0.87. Typically, Z_{RS} is below $Z_{0°C}$ by 100-300 m (Minder et al., 2011; Minder & Kingsmill, 2013; White et al., 2002; White et al., 2010), with which our model is consistent.

Hourly precipitation is then partitioned into rain and snow using estimated Z_{RS} and terrain elevation. The error term ε allows for estimation of confidence intervals (CIs) for the partitioning of rain and snow over an aggregation period (see S3). We can also compare estimated Z_{RS} against *in situ* snow depth increases.

2.7 AR return period estimation

We computed return periods of streamflow, precipitation, IVT, snowmelt, and TWI for the Feb. 2017 event against historical events. Return periods were calculated using the GEV distribution (Coles, 2001; Henn et al., 2015; Rusticucci & Tencer, 2008), which is suitable for describing the largest event from each year. GEV return periods and their CIs were estimated using MATLAB's distribution fitting implementation. The return periods for 6-10 Feb. 2017 and each of the largest events were computed for snowmelt, using the five-day cumulative decreases in daily SWE for the months of Dec. through Feb., and for TWI (the sum of snowmelt and PRISM daily precipitation interpolated to the pillow sites).

2.8 Snowmelt contribution estimation

We estimate the relative increase in TWI as a result of snowmelt, and its CI, using:

$$f_{snowmelt} = \frac{TWI - Rain}{Rain} = \frac{Snowmelt}{Rain} \quad (2).$$

Rain is estimated from the partitioned precipitation dataset. *Snowmelt* is computed as the distributed 500 m SWE map on 12 Feb. subtracted from that on 24 Jan., with new snowfall (also estimated from the partitioned precipitation dataset) from 24 Jan. to 5 Feb. added to the magnitude of the decrease in SWE between maps, in order to estimate melt over the 6-10 Feb. period alone.

3 **Results**

3.1 AR sequence and hydrologic response

In early Feb., SWE ranged from 400-1,200 mm, averaging 160% of long-term average (Figure 1b). Heavy precipitation began late on 6 Feb. into 7 Feb., the day that damage was discovered at the Oroville Dam spillway. With the spillway shut for assessment, inflows then drove an increase in reservoir storage (Figure 2a). Air temperatures remained warm on 8 Feb., as precipitation lightened. A second round of AR-driven precipitation fell from 9-10 Feb., with inflows peaking at 192,000 ft^3 s^{-1} (5,500 m^3 s^{-1}). Reservoir storage exceeded capacity and engaged the emergency spillway on 11 Feb. Ensuing damage to the spillways prompted evacuations on 12 Feb. CDWR reopened the primary spillway and storage dropped below capacity by early 13 Feb.

Observed five-day (6-10 Feb.) watershed-mean CNRFC precipitation averaged 232 mm (Figure 2b), with southwestern mid-elevations including an observation of 507 mm at Four Trees (1570 m elevation; the climatological rain-snow transition zone) where antecedent SWE was 776 mm. The AR sequence resulted in five-day average IVT generally exceeding 250 kg m^{-1} s^{-1}, a widely-used threshold of local AR conditions (Rutz et al. 2014). AR conditions reached "extreme" intensity, with an AR duration that classified it as an AR 4 on the scale of Ralph et al. (2019).

3.2 AR rain-snow elevations and precipitation partitioning

The AR precipitation was associated with anomalously high Z_{RS} over 6-10 Feb. (Figure 3a). Precipitation began on 6-7 Feb. with rain below ~1,700 m and snow above. Heavy rainfall fell at all elevations on Feb. 7. Z_{RS} persisted above 2,500 m as rain returned on 9-10 Feb., with rates exceeding 5 mm hr^{-1} at all elevations for an 8-hr period. At the highest elevations, precipitation transitioned back to snow at the end of the AR sequence. Figure 3a shows that our model for estimating Z_{RS} (based on MERRA-2 $Z_{0°C}$) qualitatively agrees with both the radar brightband heights Z_{BB}, and the *in situ* snow depth increases, which are seen only above the estimated Z_{RS}

Calculated over the 6-10 Feb. period 89% (83-93% as a 90% CI) of watershed total precipitation fell as rain (Figure 3b). 92% (85-97% CI) of precipitation fell as rain in a critical area between 1,250 and 1,750 m elevation, which comprises 56% of the watershed area and had above-normal antecedent snowpack.

The magnitude and the extent of the snowmelt is apparent in daily pillow SWE observations, with ~100 mm declines from 7 Feb. to 11 Feb. (Figure 3c), and in the comparison of satellite images taken before (24 Jan., Figure 3d) and after (12 Feb., Figure 3e) the event, in which snow cover disappeared from large portions of the watershed.

3.3 Event magnitudes and return periods: Lake Oroville inflows, precipitation, rain-snow levels, IVT, snowmelt, and TWI

Inflows to Lake Oroville were the 2nd-highest since 1987 (Figure 4a), with a 25-yr (10-112 yr CI) return period exceeded only by the Jan. 1997 flood event (Galewsky & Sobel, 2005). However, precipitation was not in the top five events with a return period of 6 yr (3-9 yr CI, Figure 4b). The Feb. 2017 event was more notable in terms of precipitation with Z_{RS} > 2,500 m (5th largest, Figure 4c). It was also the 4th-largest five-day average IVT event since 1981 (Figure 4d).

The AR sequence triggered record midwinter snowmelt at multiple snow pillows in the watershed (Figures 4e-4j). Both Four Trees (206 mm of melt) and Kettle Rock (140 mm) recorded their largest snowmelt events; the Four Trees event has a GEV return period of 223 yr (32 to >1000 yr CI). The large CI range is due to the challenge of estimating the return frequencies of an event that far exceeds the rest of the record. Four other pillows recorded the 3rd-largest melt event. Snowmelt was elevation dependent, with greater magnitudes at lower sites, *e.g.*, Four Trees at 1,570 m.

Together, the snowmelt and rainfall triggered record five-day totals of TWI calculated at the snow pillow sites (Figures 4k-4p). Kettle Rock produced its largest TWI event at 314 mm; five other sites reported TWI magnitudes among the five largest historical events, including Four Trees' 3rd-largest event at 602 mm. The large contributions of snowmelt to TWI helps to explain the discrepancy between the historical ranks of the precipitation and inflows (cf. Figures 4b and

4a). While an analysis of the other historic snowmelt events is out of scope here, their dates of occurrence suggest coincidence with known major ARs.

3.4 Watershed-wide snowmelt and contribution to TWI

The distributed SWE data provide an estimate of watershed-wide snowmelt from the Feb. 2017 event. Figure 5a shows net differences in SWE between 24 Jan. and 12 Feb. Bands of SWE loss exceeding 200 mm (consistent with Four Trees observations) are prevalent on mid-elevation slopes in the southwest of the watershed. These areas of heavy snowmelt extended into the more extensive portions of the watershed to the northeast. High-elevation areas where SWE increased by >200 mm also exist (blue). Figure 5b shows that these patterns are elevation-dependent: above 2,000 m (<10% of the watershed area), almost all areas gained SWE, while below 1,600 m, nearly all lost SWE, with the most severe losses between 1,100 and 1,400 m (nearly 20% of watershed area). No snowmelt was estimated below these elevations as they were snow-free prior to the event.

Figures 5c and 5d show the spatial distribution of TWI derived from the partitioned precipitation and mapped SWE datasets. The cumulative effects of rain and net SWE loss are evident in TWI in the southwest (Figure 5c), with the highest occurring at 1,100-1,400 m elevation (Figure 5d). Given the non-linear nature of runoff generation in such steep, complex terrain and the spatial variability of SWE loss, “hotspots” of TWI approaching 1,000 mm relatively close to Lake Oroville may have generated disproportionately high runoff.

Based on precipitation partitioning and SWE analysis, 204 mm (191-215 mm CI) of the 230 mm of precipitation fell as rain over 6-10 Feb., and snowmelt was 76 mm (53-103 mm CI). Therefore, we find that snowmelt increased TWI by 37% (25-54% CI) over rainfall alone.

4 Discussion and Conclusion

The Feb. 2017 AR sequence associated with the Oroville Dam spillways incident produced inflows to Lake Oroville that were the 2nd-largest since 1987; precipitation falling with high Z_{RS} and IVT (enhanced by warm temperatures with greater moisture content) were both the 4th-highest five-day event since 1981. Inflows were greater than the absolute precipitation magnitude would suggest; for example, the Feb. event precipitation was not even the largest of 2017 (Figure 4b). A partial explanation is that high Z_{RS} meant that nearly the entire watershed received rain (not snow) and thus produced runoff (*e.g.*, Henn et al., 2020).

Our analysis shows that deep and extensive antecedent snowpack and rainfall at most elevations led to rapid snowmelt. Large areas of the watershed experienced both melt and heavy rainfall, contributing to inflows by increasing TWI by 25-54%, a range supported by other studies of rain-on-snow floods (Guan et al., 2016; Marks et al., 2001; Mazurkiewicz et al., 2008; Musselman et al., 2018; Trubilowicz & Moore, 2017; Wayand et al., 2015).

Snowpack was unusually deep at elevations of 1,100-1,400 m (20% of the watershed) where it is typically intermittent. This was due to a colder AR sequence in Jan. that produced mostly snow. Snow cover in the climatological rain-snow transition zone indicates rain-on-snow flood risk (Wayand et al., 2015). Additionally, the Feb. AR sequence maintained warm, moist, and windy conditions for nearly four days, which would be capable of exhausting the cold content of a deep snowpack, triggering melt (Marks et al., 1998).

Antecedent soil moisture in the Lake Oroville watershed following storms in Dec. and Jan. may have also contributed to inflows (*e.g.*, Leung & Qian, 2009). However, while the limited measurements of soil moisture in the watershed prevent a systematic evaluation, they indicate that soils had been draining, *i.e.*, no soil water inputs, for at least three weeks before the

Feb. 2017 event (Avanzi et al., 2018; their Figure 5). The weather in that period was predominantly dry or featured with relatively low Z_{RS}, such that most of the watershed received snow, not rain, and soil moisture would not have increased. These observations suggest that soil moisture anomalies – beyond normal seasonal increases during winter– were not a driver.

That the event precipitation totals were lower than other historical floods in the Lake Oroville watershed suggests that a similar AR with higher precipitation totals could have produced a more catastrophic flood. Research has suggested that in the Sierra Nevada warm AR events have become more common (Hatchett et al., 2017), winter snowmelt rates are increasing (Kapnick & Hall, 2011), and anthropogenic climate change may drive the region towards more extreme ARs (Gershunov et al., 2019; Swain et al., 2018). Thus, extreme melt driven by rain-on-snow events may become more common, even as snowpack recedes in maritime climates due to warming temperatures (Musselman et al., 2018). The AR sequence in this study may be indicative of this type of rain-on-snow flood.

Monitoring snowpack across a wider range of elevations may provide insight into rain-on-snow flood risk. The CDWR snow pillow stations are situated at elevations of 1,500-2,600 m where snowpack generally persists into the spring, but these elevations represent <50% of Lake Oroville's watershed area. Four Trees is the lowest snow pillow (1,570 m elevation) and it recorded dramatically more snowmelt (Figures 4e and 5b) than other sites. The distributed SWE product, which leverages information from 114 regional snow pillows and satellite observations, indicated that the greatest melt occurred at elevations below Four Trees and above 1,000 m. This elevation band comprises ~37% of the basin area (Figure 1b) and produced ~70% of the basin-wide snowmelt, but *in situ* snow observations are unavailable here.

Our examination of the AR sequence during the Oroville Dam spillways incident suggests that snowmelt driven by high Z_{RS} and warm temperatures may explain the discrepancy in historical return frequencies between the observed runoff and precipitation. The spillways incident was likely exacerbated by the AR-driven extreme snowmelt. Our findings highlight the risk to public safety and infrastructure associated with warming temperatures in observational evidence and in projections of climate change.

Acknowledgments

BH and FMR were supported by CDWR Atmospheric River Research program grant 4600010378 TO#15 Am 22. KM, NM and LL were supported by NASA Applied Sciences Water Resources Program under grant NNX17AF50G. Tessa Maurer and Francisco Avanzi shared snow depth observations from the University of California's Feather River Hydrologic Observatory, and Brian Kawzenuk provided IVT maps. Data used in this paper are available at the sources indicated or are hosted at ftp://snowserver.colorado.edu/pub/AGU.

Figure Captions

Figure 1. a) Topographic map of the watershed of the Feather River above Lake Oroville. b) Elevation-area cumulative distribution of the watershed (black line, lower x axis), showing 10%, median, and 90% cumulative elevations (red lines). The elevations of the snow courses and pillows are also plotted against early Feb. 2017 SWE observations (upper x axis).

Figure 2. a) Hydrologic summary of the Feb. 2017 AR sequence: Lake Oroville inflows, outflows, storage, and water surface elevation. Thin dotted red line indicates the elevation of emergency spillway. b) Precipitation accumulations over 6-10 Feb. 2017; Four Trees snow pillow shown with black circle. c) Atmospheric IVT magnitude (shading) averaged over 0Z 7 Feb. to 0Z 11 Feb. 2017, with IVT vectors overlaid.

Figure 3. a) Precipitation (shading) vs. watershed elevation over 6-10 Feb. 2017. Z_{RS} estimated from MERRA-2 (heavy dashes) with 90% CI (thin dashes) are shown. Observed Oroville radar brightband heights and in situ snow depth increases against the sites' elevations are also plotted. b) Fraction of watershed precipitation over 6-10 Feb. falling as rain, averaged by elevation (heavy line) along with 90% CI (dashed lines). c) Difference in SWE relative to 7 Feb. at 6 snow pillows with the greatest declines in SWE. d) and e) MODIS satellite images of snow cover before (24 Jan.) and after (12 Feb.) the AR sequence.

Figure 4. Historical storm magnitudes and GEV return periods; magnitudes are on the left axis and return periods on the right. return period 90% CI indicated by vertical error bars. The top historical events are shown with the 6-10 Feb. 2017 event highlighted. a) Five-day inflow volumes. b) Precipitation. c) Precipitation falling with a rain-snow level above 2,500 m. d) IVT (five-day average). e) - j) Snowmelt at snow pillows. k) - j) TWI at snow pillows.

Figure 5. a) Change in SWE over the Lake Oroville watershed from 24 Jan. to 12 Feb. 2017. Snow pillow shown with diamond symbols. b) Boxplots of change in SWE by elevation bin; change recorded at snow pillows shown with circled diamonds. c) 6-10 Feb. TWI over the watershed. d) Boxplots of event TWI and rainfall only.

References

Avanzi, F., Maurer, T., Malek, S., Glaser, S., Bales, R., & Conklin, M. (2018). *Feather River Hydrologic Observatory: Improving Hydrological Snowpack Forecasting for Hydropower Generation Using Intelligent Information Systems*.

Coles, S. (2001). *An Introduction to Statistical Modeling of Extreme Values*. London: Springer London. https://doi.org/10.1007/978-1-4471-3675-0

Daly, C., Neilson, R., & Phillips, D. (1994). A statistical-topographic model for mapping climatological precipitation over mountainous terrain. *Journal of Applied Meteorology*, *33*. Retrieved from http://journals.ametsoc.org/doi/abs/10.1175/1520-0450(1994)033%3C0140:ASTMFM%3E2.0.CO;2

France, J. W., Alvi, I. A., Dickson, P. A., Falvey, H. T., Rigbey, S. J., & Trojanowski, J. (2018). Independent Forensic Team Report: Oroville Dam Spillway Incident, 1–584.

Galewsky, J., & Sobel, A. (2005). Moist dynamics and orographic precipitation in northern and central California during the New Year's flood of 1997. *Monthly Weather Review*, 1594–1612. Retrieved from http://journals.ametsoc.org/doi/abs/10.1175/MWR2943.1

Gelaro, R., McCarty, W., Suárez, M. J., Todling, R., Molod, A., Takacs, L., et al. (2017). The modern-era retrospective analysis for research and applications, version 2 (MERRA-2). *Journal of Climate*, *30*(14), 5419–5454. https://doi.org/10.1175/JCLI-D-16-0758.1

Gershunov, A., Shulgina, T., Clemesha, R. E. S., Guirguis, K., Pierce, D. W., Dettinger, M. D., et al. (2019). Precipitation regime change in Western North America: The role of Atmospheric Rivers. *Scientific Reports*, *9*(1), 9944. https://doi.org/10.1038/s41598-019-46169-w

Guan, B., Waliser, D. E., Ralph, F. M., Fetzer, E. J., & Neiman, P. J. (2016). Hydrometeorological Characteristics of Rain-on-Snow Events Associated with Atmospheric Rivers. *Geophysical Research Letters*, n/a-n/a. https://doi.org/10.1002/2016GL067978

Hatchett, B., Daudert, B., Garner, C., Oakley, N., Putnam, A., & White, A. (2017). Winter Snow Level Rise in the Northern Sierra Nevada from 2008 to 2017. *Water*, *9*(11), 899. https://doi.org/10.3390/w9110899

Henn, B., Cao, Q., Lettenmaier, D. P., Magirl, C. S., Mass, C., Brent Bower, J., et al. (2015). Hydroclimatic Conditions Preceding the March 2014 Oso Landslide*. *Journal of Hydrometeorology*, *16*(3), 1243–1249. https://doi.org/10.1175/JHM-D-15-0008.1

Henn, B., Weihs, R., Martin, A. C., Ralph, F. M., & Osborne, T. C. (2020). Skill of rain-snow level forecasts for landfalling atmospheric rivers : A multi-model model assessment using California's network of vertically profiling radars. *Journal of Hydrometeorology*. https://doi.org/10.1175/JHM-D-18-0212

Jackson, D. L., Hughes, M., & Wick, G. A. (2016). Evaluation of landfalling atmospheric rivers along the U.S. West Coast in reanalysis data sets. *Journal of Geophysical Research: Atmospheres*, *121*(6), 2705–2718. https://doi.org/10.1002/2015JD024412

Kapnick, S., & Hall, A. (2011). Causes of recent changes in western North American snowpack.

Climate Dynamics, *38*(9–10), 1885–1899. https://doi.org/10.1007/s00382-011-1089-y

Leung, L. R., & Qian, Y. (2009). Atmospheric rivers induced heavy precipitation and flooding in the western U.S. simulated by the WRF regional climate model. *Geophysical Research Letters*, *36*(3), n/a-n/a. https://doi.org/10.1029/2008GL036445

Lin, Y., & Mitchell, K. E. (2005). The NCEP Stage II/IV hourly precipitation analyses: development and applications. *Preprints, 19th Conf. on Hydrology, American Meteorological Society, San Diego, CA, 9-13 January 2005, Paper 1.2*, 2–5. Retrieved from http://www.emc.ncep.noaa.gov/mmb/ylin/pcpanl/refs/stage2-4.19hydro.pdf

Lundquist, J. D., Neiman, P. J., Martner, B., White, A. B., Gottas, D. J., & Ralph, F. M. (2008). Rain versus Snow in the Sierra Nevada, California: Comparing Doppler Profiling Radar and Surface Observations of Melting Level. *Journal of Hydrometeorology*, *9*(2), 194–211. https://doi.org/10.1175/2007JHM853.1

Marks, D., Kimball, J., Tingey, D., & Link, T. (1998). The sensitivity of snowmelt processes to climate conditions and forest cover during rain-on-snow: a case study of the 1996 Pacific Northwest flood. *Hydrological Processes*, *12*(10–11), 1569–1587. https://doi.org/10.1002/(SICI)1099-1085(199808/09)12:10/11<1569::AID-HYP682>3.0.CO;2-L

Marks, D., Link, T., Winstral, A., & Garen, D. (2001). Simulating snowmelt processes during rain-on-snow over a semi-arid mountain basin. *Annals of Glaciology*, *32*, 195–202.

Mazurkiewicz, A. B., Callery, D. G., & McDonnell, J. J. (2008). Assessing the controls of the snow energy balance and water available for runoff in a rain-on-snow environment. *Journal of Hydrology*, *354*(1–4), 1–14. https://doi.org/10.1016/j.jhydrol.2007.12.027

Minder, J. R., & Kingsmill, D. E. (2013). Mesoscale Variations of the Atmospheric Snow Line over the Northern Sierra Nevada: Multiyear Statistics, Case Study, and Mechanisms. *Journal of the Atmospheric Sciences*, *70*(3), 916–938. https://doi.org/10.1175/JAS-D-12-0194.1

Minder, J. R., Durran, D. R., & Roe, G. H. (2011). Mesoscale Controls on the Mountainside Snow Line. *Journal of the Atmospheric Sciences*, *68*(9), 2107–2127. https://doi.org/10.1175/JAS-D-10-05006.1

Musselman, K. N., Molotch, N. P., & Margulis, S. A. (2017). Snowmelt response to simulated warming across a large elevation gradient, southern Sierra Nevada, California. *The Cryosphere*, *11*(6), 2847–2866. https://doi.org/10.5194/tc-11-2847-2017

Musselman, K. N., Lehner, F., Ikeda, K., Clark, M. P., Prein, A. F., Liu, C., et al. (2018). Projected increases and shifts in rain-on-snow flood risk over western North America. *Nature Climate Change*, *8*(9), 808–812. https://doi.org/10.1038/s41558-018-0236-4

Ralph, F. M., & Dettinger, M. D. (2012). Historical and national perspectives on extreme west coast precipitation associated with atmospheric rivers during december 2010. *Bulletin of the American Meteorological Society*, *93*(6), 783–790. https://doi.org/10.1175/BAMS-D-11-00188.1

Ralph, F. Martin, Neiman, P. J., & Wick, G. a. (2004). Satellite and CALJET Aircraft

Observations of Atmospheric Rivers over the Eastern North Pacific Ocean during the Winter of 1997/98. *Monthly Weather Review*, *132*(7), 1721–1745. https://doi.org/10.1175/1520-0493(2004)132<1721:SACAOO>2.0.CO;2

Ralph, F. Martin, Neiman, P. J., & Rotunno, R. (2005). Dropsonde Observations in Low-Level Jets over the Northeastern Pacific Ocean from CALJET-1998 and PACJET-2001: Mean Vertical-Profile and Atmospheric-River Characteristics. *Monthly Weather Review*, *133*(4), 889–910. https://doi.org/10.1175/MWR2896.1

Ralph, F. Martin, Cordeira, J. M., Neiman, P. J., & Hughes, M. (2016). Landfalling Atmospheric Rivers, the Sierra Barrier Jet, and Extreme Daily Precipitation in Northern California's Upper Sacramento River Watershed. *Journal of Hydrometeorology*, *17*(7), 1905–1914. https://doi.org/10.1175/JHM-D-15-0167.1

Ralph, F. Martin, Rutz, J. J., Cordeira, J. M., Dettinger, M., Anderson, M., Reynolds, D., et al. (2019). A scale to characterize the strength and impacts of atmospheric rivers. *Bulletin of the American Meteorological Society*, *100*(2), 269–289. https://doi.org/10.1175/BAMS-D-18-0023.1

Rusticucci, M., & Tencer, B. (2008). Observed changes in return values of annual temperature extremes over Argentina. *Journal of Climate*, *21*(21), 5455–5467. https://doi.org/10.1175/2008JCLI2190.1

Rutz, J. J., Steenburgh, W. J., & Ralph, F. M. (2014). Climatological characteristics of atmospheric rivers and their inland penetration over the western United States. *Monthly Weather Review*, *142*(February 2006), 905–921. https://doi.org/10.1175/MWR-D-13-00168.1

Schneider, D., & Molotch, N. P. (2016). Real-time estimation of snow water equivalent in the Upper Colorado River Basin using MODIS-based SWE Reconstructions and SNOTEL data. *Water Resources Research*, *52*(10), 7892–7910. https://doi.org/10.1002/2016WR019067

Swain, D. L., Langenbrunner, B., Neelin, J. D., & Hall, A. (2018). Increasing precipitation volatility in twenty-first-century California. *Nature Climate Change*, *8*(5), 427–433. https://doi.org/10.1038/s41558-018-0140-y

Trubilowicz, J. W., & Moore, R. D. (2017). Quantifying the role of the snowpack in generating water available for run-off during rain-on-snow events from snow pillow records. *Hydrological Processes*, *31*(23), 4136–4150. https://doi.org/10.1002/hyp.11310

Vano, J. A., Dettinger, M. D., Cifelli, R., Curtis, D., Dufour, A., Miller, K., et al. (2019). Hydroclimatic extremes as challenges for the water management community: Lessons from oroville dam and hurricane harvey. *Bulletin of the American Meteorological Society*, *100*(1), S9–S14. https://doi.org/10.1175/BAMS-D-18-0219.1

Wayand, N. E., Lundquist, J. D., & Clark, M. P. (2015). Modeling the influence of hypsometry, vegetation, and storm energy on snowmelt contributions to basins during rain-on-snow floods. *Water Resources Research*, 8551–8569. https://doi.org/10.1002/2014WR016576

White, A. B., Anderson, M. L., Dettinger, M. D., Ralph, F. M., Hinojosa, A., Cayan, D. R., et al. (2013). A Twenty-First-Century California Observing Network for Monitoring Extreme

Weather Events. *Journal of Atmospheric and Oceanic Technology*, *30*(8), 1585–1603. https://doi.org/10.1175/JTECH-D-12-00217.1

White, Allen B., Gottas, D. J., Strem, E. T., Ralph, F. M., & Neiman, P. J. (2002). An automated brightband height detection algorithm for use with Doppler radar spectral moments. *Journal of Atmospheric and Oceanic Technology*, *19*(5), 687–697. https://doi.org/10.1175/1520-0426(2002)019<0687:AABHDA>2.0.CO;2

White, Allen B., Moore, B. J., Gottas, D. J., & Neiman, P. J. (2019). Winter Storm Conditions Leading to Excessive Runoff above California's Oroville Dam during January and February 2017. *Bulletin of the American Meteorological Society*, *100*(1), 55–70. https://doi.org/10.1175/BAMS-D-18-0091.1

White, Allen B, Gottas, D. J., Henkel, A. F., Neiman, P. J., Ralph, F. M., & Gutman, S. I. (2010). Developing a Performance Measure for Snow-Level Forecasts. *Journal of Hydrometeorology*, *11*(3), 739–753. https://doi.org/10.1175/2009JHM1181.1

Xia, Y., Mitchell, K., Ek, M., Cosgrove, B., Sheffield, J., Luo, L., et al. (2012). Continental-scale water and energy flux analysis and validation for North American Land Data Assimilation System project phase 2 (NLDAS-2): 2. Validation of model-simulated streamflow. *Journal of Geophysical Research*, *117*, D03110. https://doi.org/10.1029/2011JD016051

Supporting References

Bretherton, C. S., Widmann, M., Dymnikov, V. P., Wallace, J. M., & Bladé, I. (1999). The effective number of spatial degrees of freedom of a time-varying field. *Journal of Climate*, 12(7), 1990–2009. https://doi.org/10.1175/1520-0442(1999)012<1990:TENOSD>2.0.CO;2

Guan, B., Molotch, N. P., Waliser, D. E., Fetzer, E. J., & Neiman, P. J. (2013). The 2010/2011 snow season in California's Sierra Nevada: Role of atmospheric rivers and modes of large-scale variability. *Water Resources Research*, 49(10), 6731–6743. https://doi.org/10.1002/wrcr.20537

Lin, Y., & Mitchell, K. E. (2005). The NCEP Stage II/IV hourly precipitation analyses: development and applications. Preprints, *19th Conf. on Hydrology*, American Meteorological Society, San Diego, CA, 9-13 January 2005, Paper 1.2, 2–5. Retrieved from http://www.emc.ncep.noaa.gov/mmb/ylin/pcpanl/refs/stage2-4.19hydro.pdf

Molotch, N. P., Colee, M. T., Bales, R. C., & Dozier, J. (2005). Estimating the spatial distribution of snow water equivalent in an alpine basin using binary regression tree models: the impact of digital elevation data and independent variable selection. *Hydrological Processes*, 19(7), 1459–1479. https://doi.org/10.1002/hyp.5586

Molotch, Noah P. (2009). Reconstructing snow water equivalent in the Rio Grande headwaters using remotely sensed snow cover data and a spatially distributed snowmelt model. *Hydrological Processes*, 23(7), 1076–1089. https://doi.org/10.1002/hyp.7206

Painter, T. H., Rittger, K., McKenzie, C., Slaughter, P., Davis, R. E., & Dozier, J. (2009). Retrieval of subpixel snow covered area, grain size, and albedo from MODIS. *Remote Sensing of Environment*, 113(4), 868–879. https://doi.org/10.1016/j.rse.2009.01.001

Schneider, D., & Molotch, N. P. (2016). Real-time estimation of snow water equivalent in the Upper Colorado River Basin using MODIS-based SWE Reconstructions and SNOTEL data. *Water Resources Research*, 52(10), 7892–7910. https://doi.org/10.1002/2016WR019067

Xia, Y., Mitchell, K., Ek, M., Cosgrove, B., Sheffield, J., Luo, L., et al. (2012). Continental-scale water and energy flux analysis and validation for North American Land Data Assimilation System project phase 2 (NLDAS-2): 2. Validation of model-simulated streamflow. *Journal of Geophysical Research Atmospheres*, 117(3), 1–23. https://doi.org/10.1029/2011JD016051

Figures

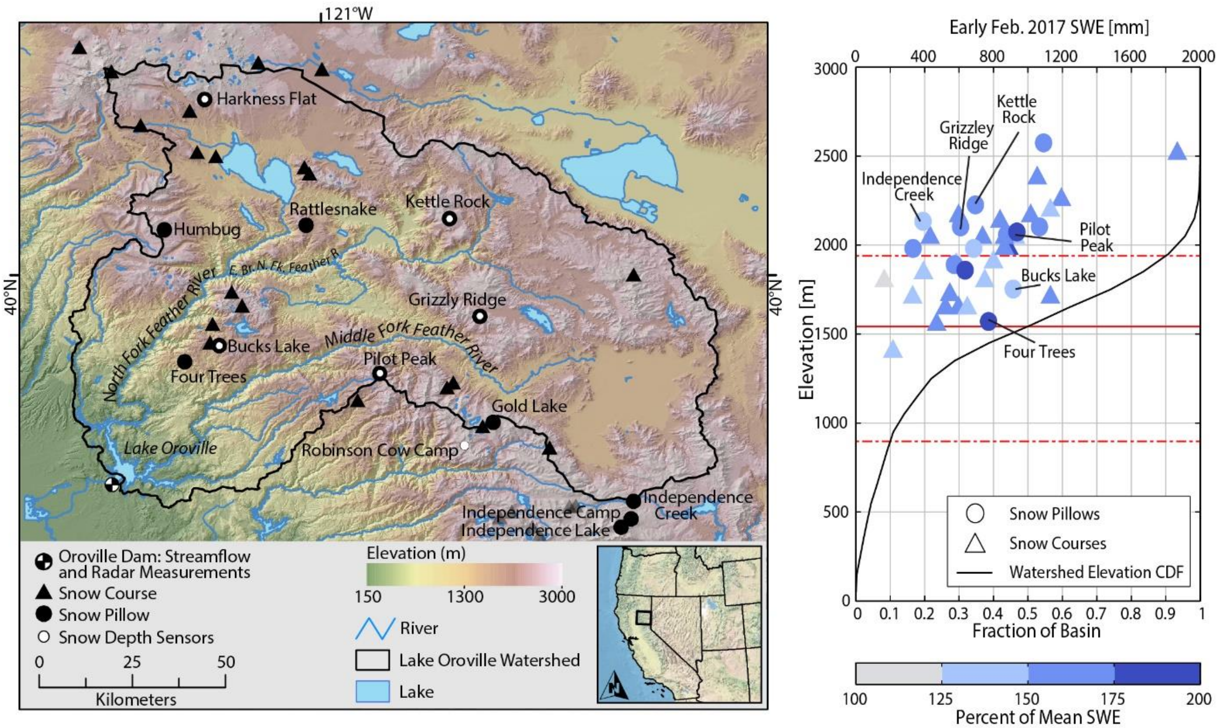

Figure 1. a) Topographic map of the watershed of the Feather River above Lake Oroville. b) Elevation-area cumulative distribution of the watershed (black line, lower x axis), showing 10%, median, and 90% cumulative elevations (red lines). The elevations of the snow courses and pillows are also plotted against early Feb. 2017 SWE observations (upper x axis).

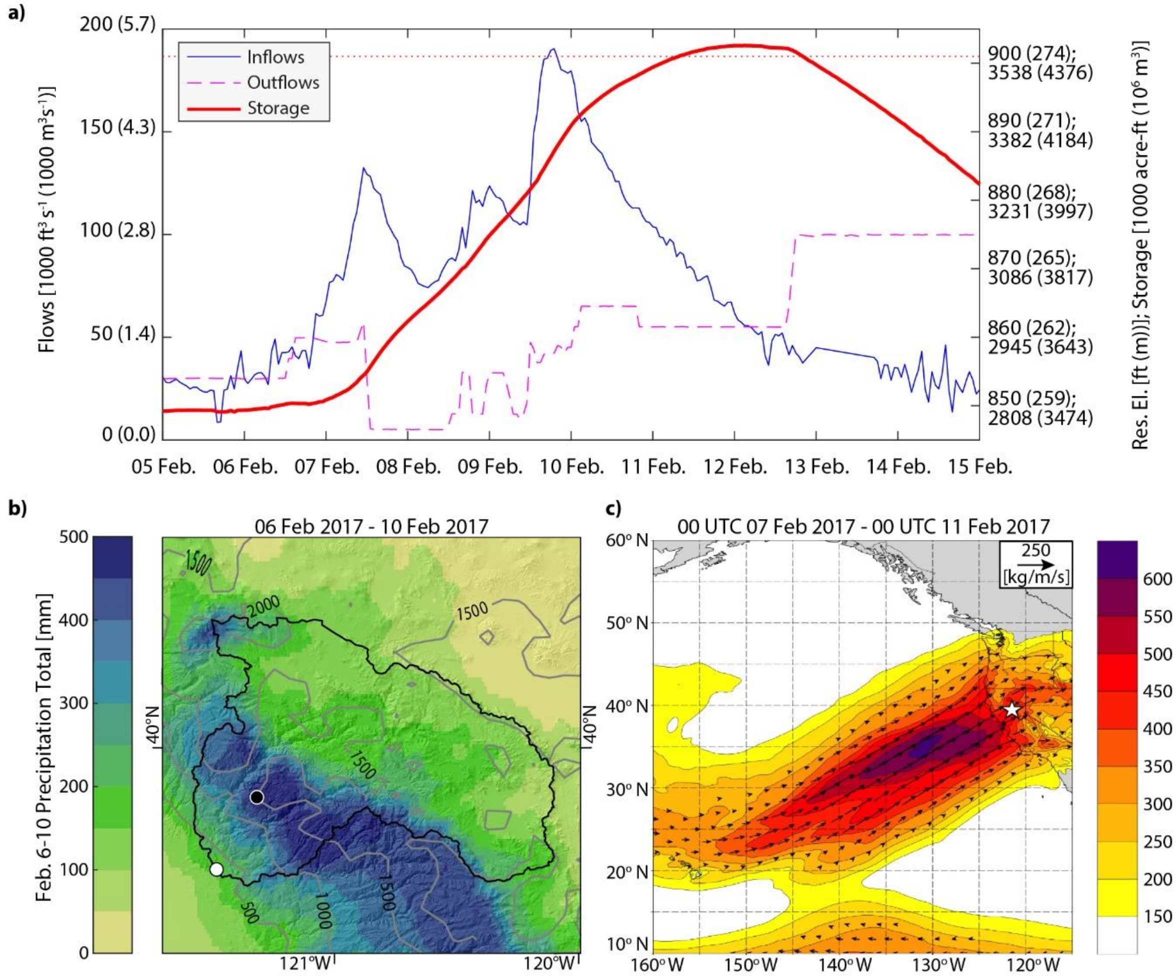

Figure 2. a) Hydrologic summary of the Feb. 2017 AR sequence: Lake Oroville inflows, outflows, storage, and water surface elevation. Thin dotted red line indicates the elevation of emergency spillway. b) Precipitation accumulations over 6-10 Feb. 2017; Four Trees snow pillow shown with black circle. c) Atmospheric IVT magnitude (shading) averaged over 0Z 7 Feb. to 0Z 11 Feb. 2017, with IVT vectors overlaid.

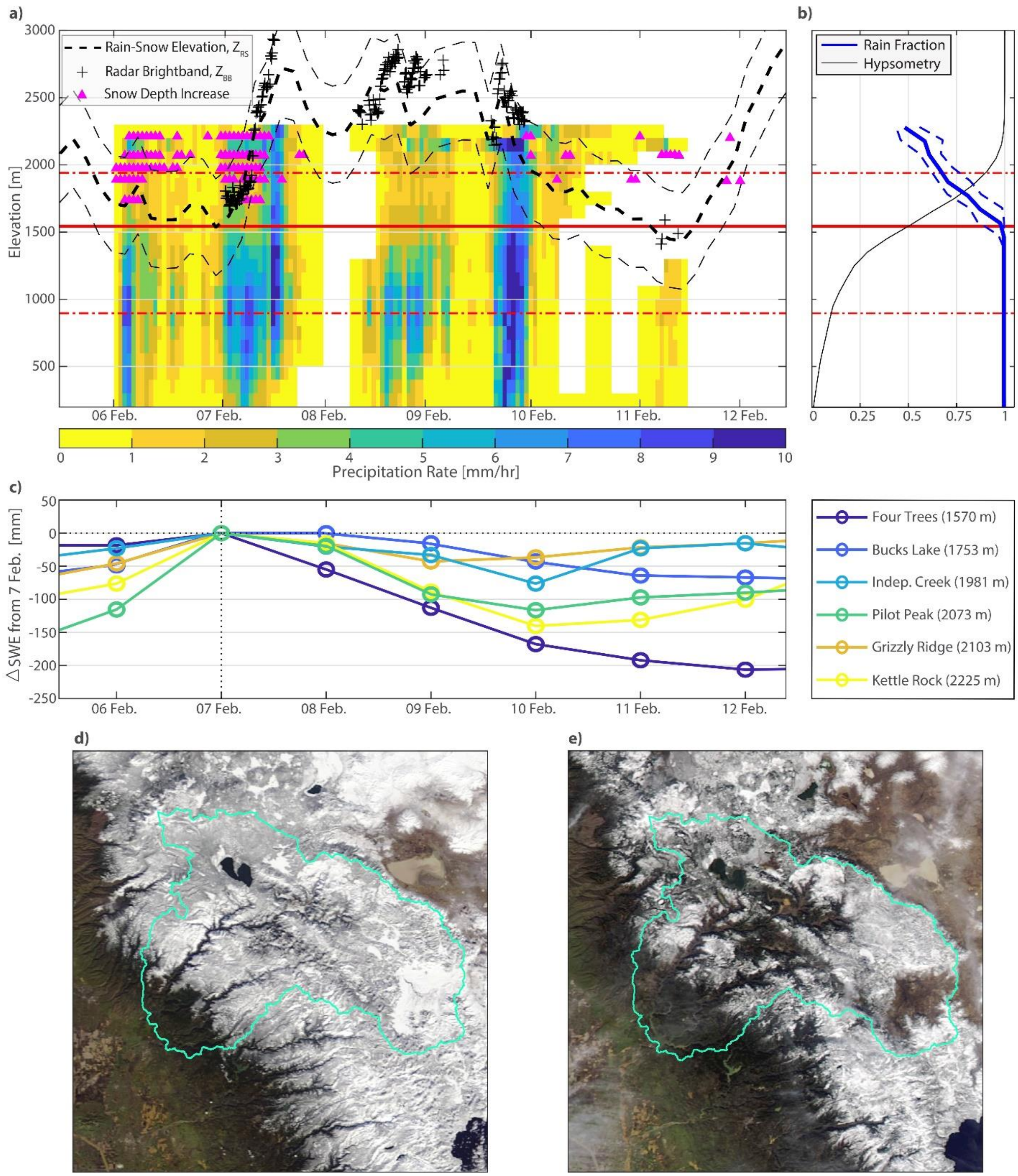

Figure 3. a) Precipitation (shading) vs. watershed elevation over 6-10 Feb. 2017. Z_{RS} estimated from MERRA-2 (heavy dashes) with 90% CI (thin dashes) are shown. Observed Oroville radar brightband heights and in situ snow depth increases against the sites' elevations are also plotted. b) Fraction of watershed precipitation over 6-10 Feb. falling as rain, averaged by elevation (heavy line) along with 90% CI (dashed lines). c) Difference in SWE relative to 7 Feb. at 6 snow

pillows with the greatest declines in SWE. d) and e) MODIS satellite images of snow cover before (24 Jan.) and after (12 Feb.) the AR sequence.

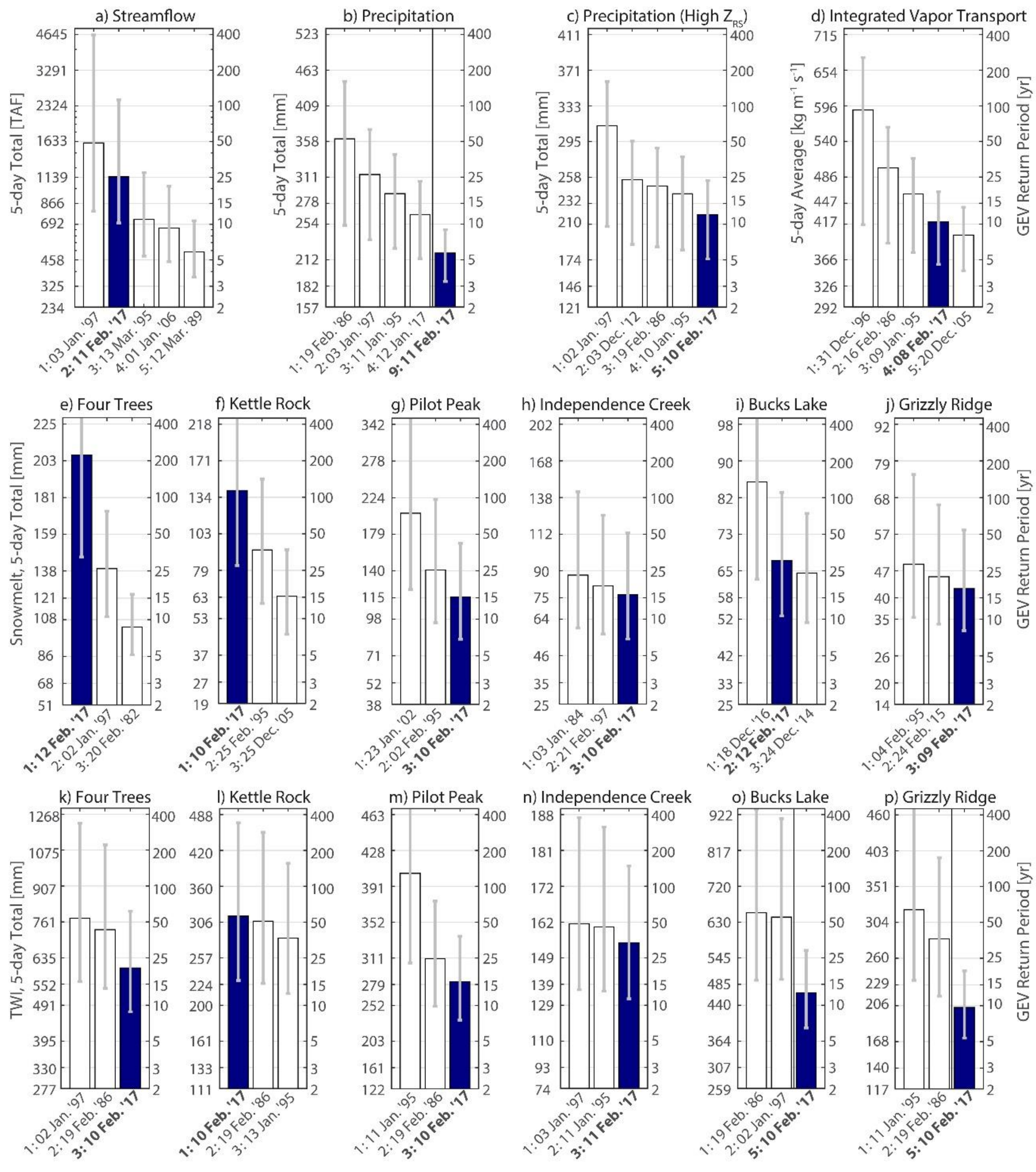

Figure 4. Historical storm magnitudes and GEV return periods; magnitudes are on the left axis and return periods on the right. return period 90% CI indicated by vertical error bars. The top historical events are shown with the 6-10 Feb. 2017 event highlighted. a) Five-day inflow volumes. b) Precipitation. c) Precipitation falling with a rain-snow level above 2,500 m. d) IVT (five-day average). e) - j) Snowmelt at snow pillows. k) - j) TWI at snow pillows.

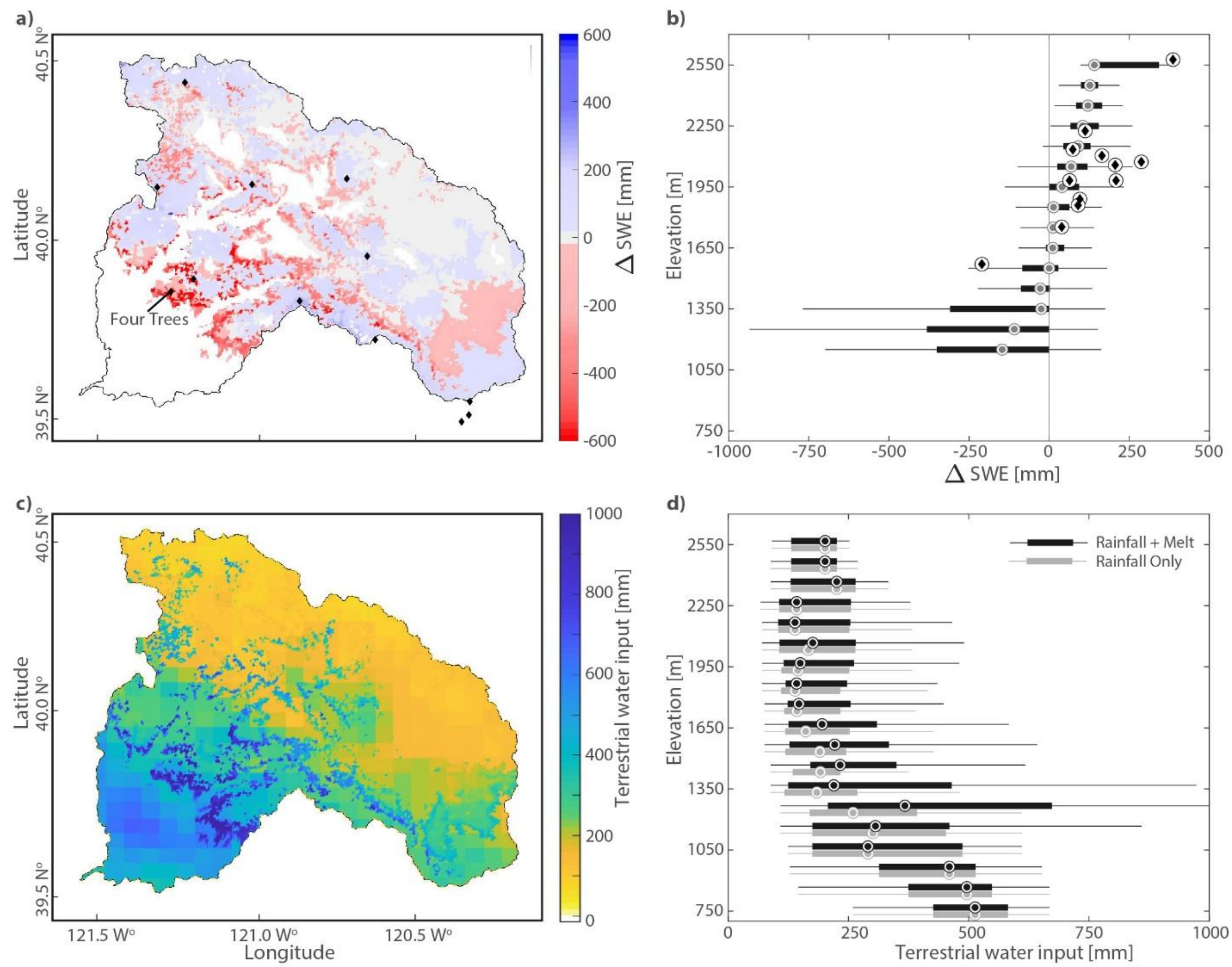

Figure 5. a) Change in SWE over the Lake Oroville watershed from 24 Jan. to 12 Feb. 2017. Snow pillow shown with diamond symbols. b) Boxplots of change in SWE by elevation bin; change recorded at snow pillows shown with circled diamonds. c) 6-10 Feb. TWI over the watershed. d) Boxplots of event TWI and rainfall only.

Figure 1.

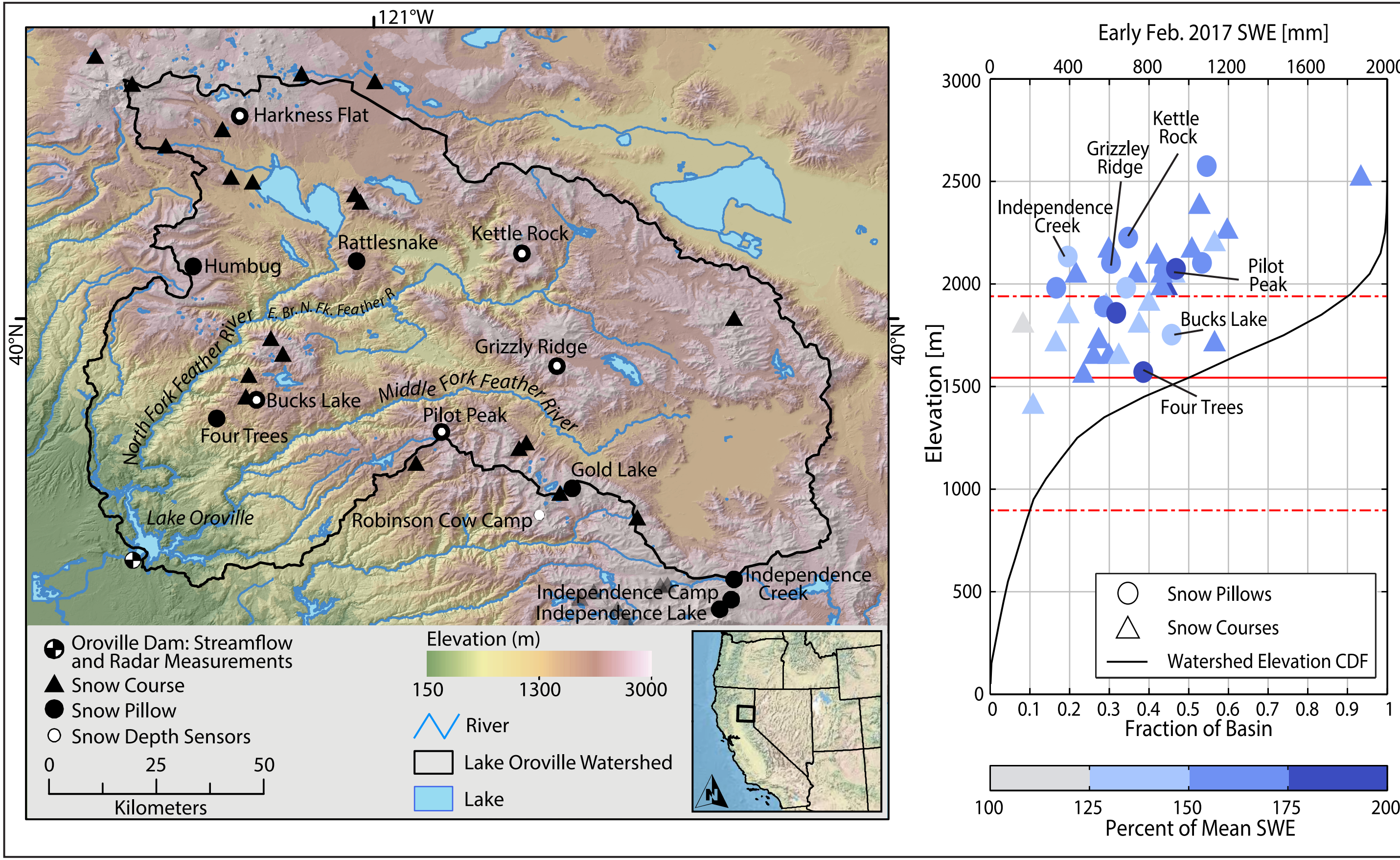
121°W
40°N
40°N
Harkness Flat
Humbug
Rattlesnake
Kettle Rock
E. Br. N. Fk. Feather R.
North Fork Feather River
Grizzly Ridge
Bucks Lake
Four Trees
Middle Fork Feather River
Pilot Peak
Gold Lake
Lake Oroville
Robinson Cow Camp
Independence Creek
Independence Camp
Independence Lake
Oroville Dam: Streamflow and Radar Measurements
Snow Course
Snow Pillow
Snow Depth Sensors
0 25 50
Kilometers
Elevation (m)
150 1300 3000
River
Lake Oroville Watershed
Lake
Early Feb. 2017 SWE [mm]
0 400 800 1200 1600 2000
Elevation [m]
3000 2500 2000 1500 1000 500 0
Kettle Rock
Grizzley Ridge
Independence Creek
Pilot Peak
Bucks Lake
Four Trees
Snow Pillows
Snow Courses
Watershed Elevation CDF
0 0.1 0.2 0.3 0.4 0.5 0.6 0.7 0.8 0.9 1
Fraction of Basin
100 125 150 175 200
Percent of Mean SWE

Figure 2.

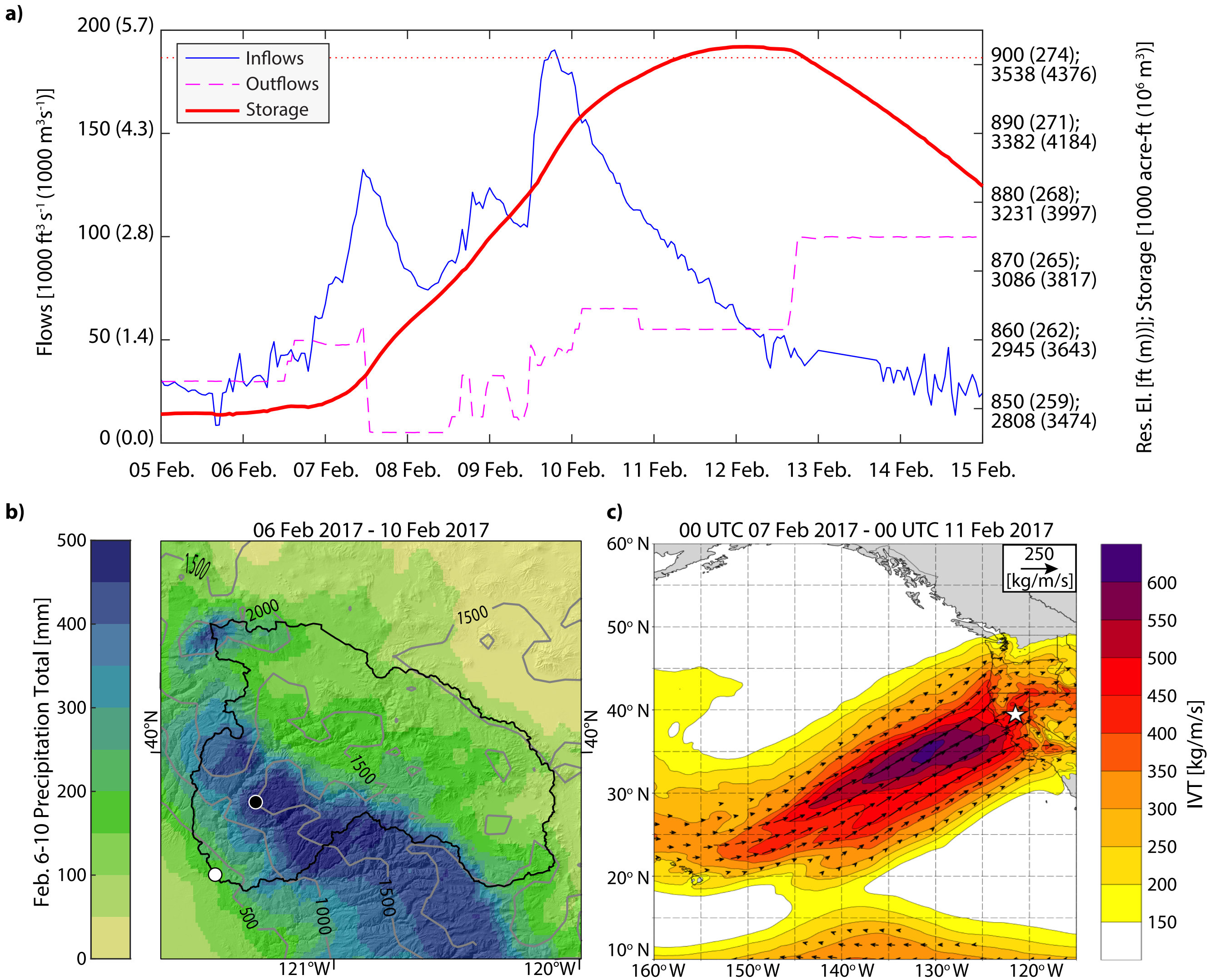
a)
Inflows
Outflows
Storage
Flows [1000 ft^3 s^{-1} (1000 m^{3}s^{-1})]
200 (5.7)
150 (4.3)
100 (2.8)
50 (1.4)
0 (0.0)
900 (274); 3538 (4376)
890 (271); 3382 (4184)
880 (268); 3231 (3997)
870 (265); 3086 (3817)
860 (262); 2945 (3643)
850 (259); 2808 (3474)
Res. El. [ft (m)]; Storage [1000 acre-ft (10^6 m^3)]
05 Feb. 06 Feb. 07 Feb. 08 Feb. 09 Feb. 10 Feb. 11 Feb. 12 Feb. 13 Feb. 14 Feb. 15 Feb.
b)
06 Feb 2017 - 10 Feb 2017
Feb. 6-10 Precipitation Total [mm]
500 400 300 200 100 0
1500
2000
1500
1500
500
1000
1500
40°N
121°W
120°W
c)
00 UTC 07 Feb 2017 - 00 UTC 11 Feb 2017
250 [kg/m/s]
60° N 50° N 40° N 30° N 20° N 10° N
160° W 150° W 140° W 130° W 120° W
600 550 500 450 400 350 300 250 200 150
IVT [kg/m/s]

Figure 3.

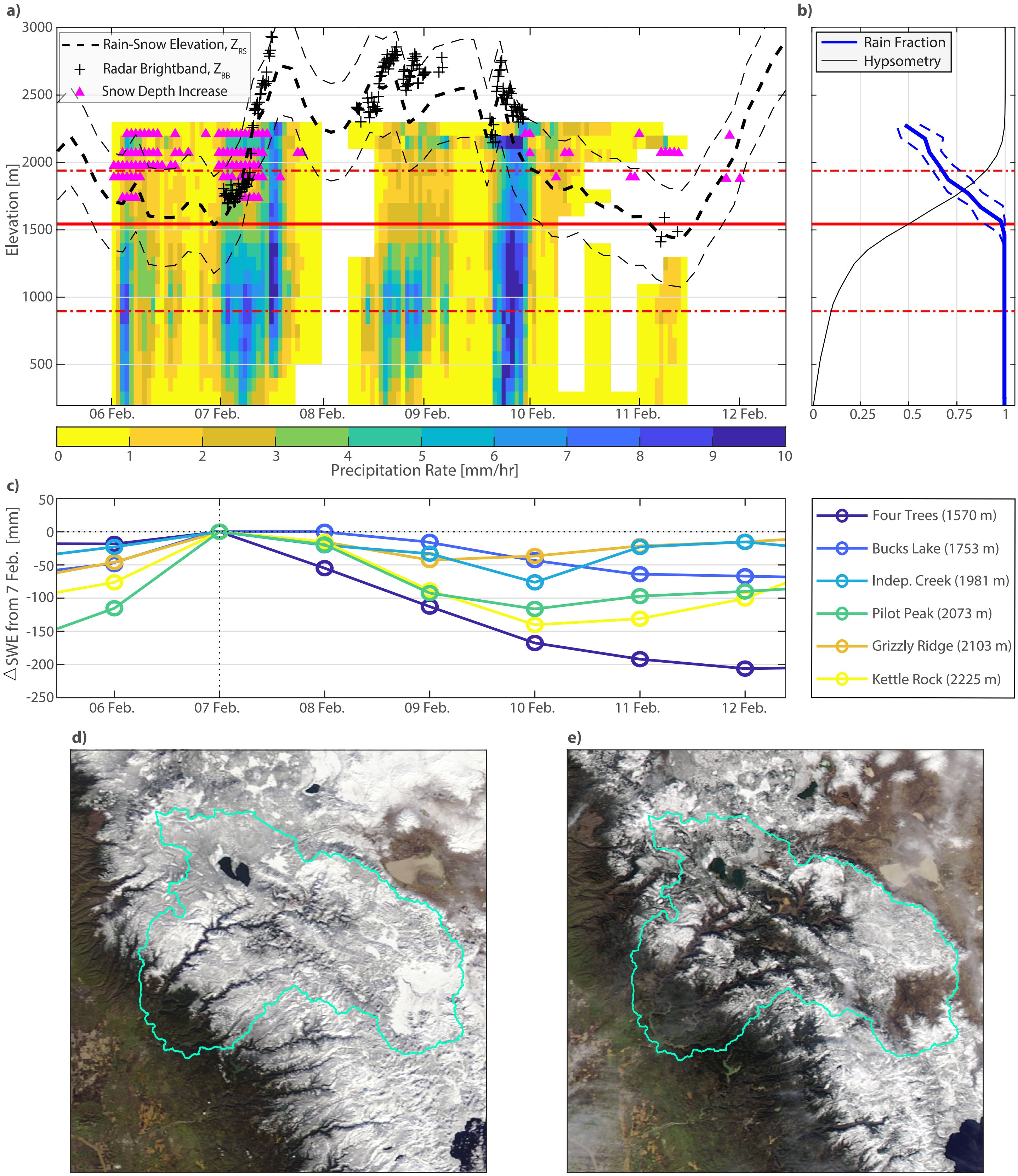

a)
b)
Rain-Snow Elevation, Z_{RS}
Radar Brightband, Z_{BB}
Snow Depth Increase
Elevation [m]
3000
2500
2000
1500
1000
500
06 Feb.
07 Feb.
08 Feb.
09 Feb.
10 Feb.
11 Feb.
12 Feb.
Rain Fraction
Hypsometry
0
0.25
0.5
0.75
1
Precipitation Rate [mm/hr]
0 1 2 3 4 5 6 7 8 9 10
c)
ΔSWE from 7 Feb. [mm]
50
0
-50
-100
-150
-200
-250
Four Trees (1570 m)
Bucks Lake (1753 m)
Indep. Creek (1981 m)
Pilot Peak (2073 m)
Grizzly Ridge (2103 m)
Kettle Rock (2225 m)
d)
e)

Figure 4.

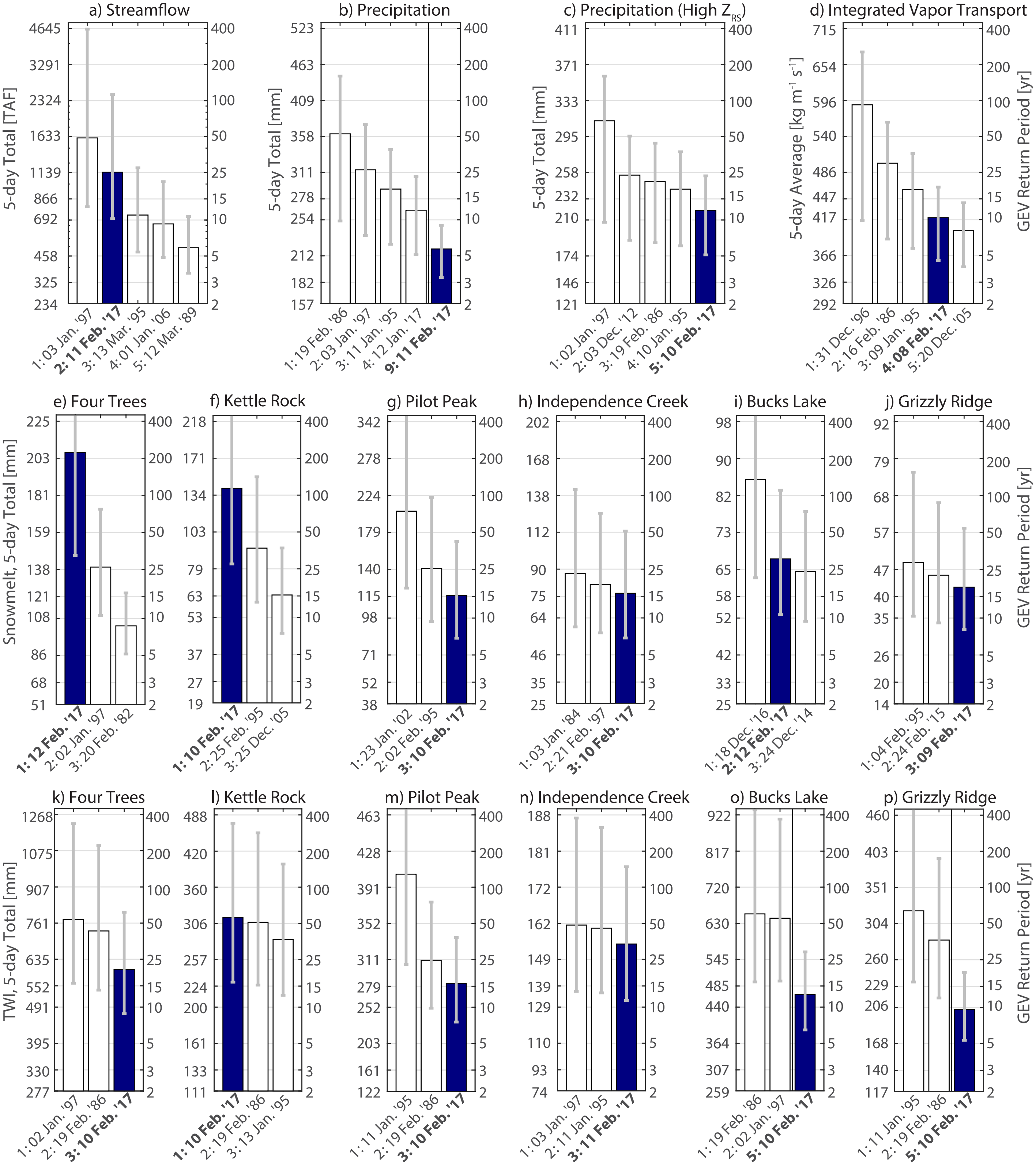
a) Streamflow
5-day Total [TAF]
1: 03 Jan. '97
2: 11 Feb. '17
3: 13 Mar. '95
4: 01 Jan. '06
5: 12 Mar. '89
b) Precipitation
5-day Total [mm]
1: 19 Feb. '86
2: 03 Jan. '97
3: 11 Jan. '95
4: 12 Jan. '17
9: 11 Feb. '17
c) Precipitation (High Z_{RS})
1: 02 Jan. '97
2: 03 Dec. '12
3: 19 Feb. '86
4: 10 Jan. '95
5: 10 Feb. '17
d) Integrated Vapor Transport
5-day Average [kg m^{-1} s^{-1}]
GEV Return Period [yr]
1: 31 Dec. '96
2: 16 Feb. '86
3: 09 Jan. '95
4: 08 Feb. '17
5: 20 Dec. '05
e) Four Trees
f) Kettle Rock
g) Pilot Peak
h) Independence Creek
i) Bucks Lake
j) Grizzly Ridge
Snowmelt, 5-day Total [mm]
k) Four Trees
l) Kettle Rock
m) Pilot Peak
n) Independence Creek
o) Bucks Lake
p) Grizzly Ridge
TWI, 5-day Total [mm]

Figure 5.

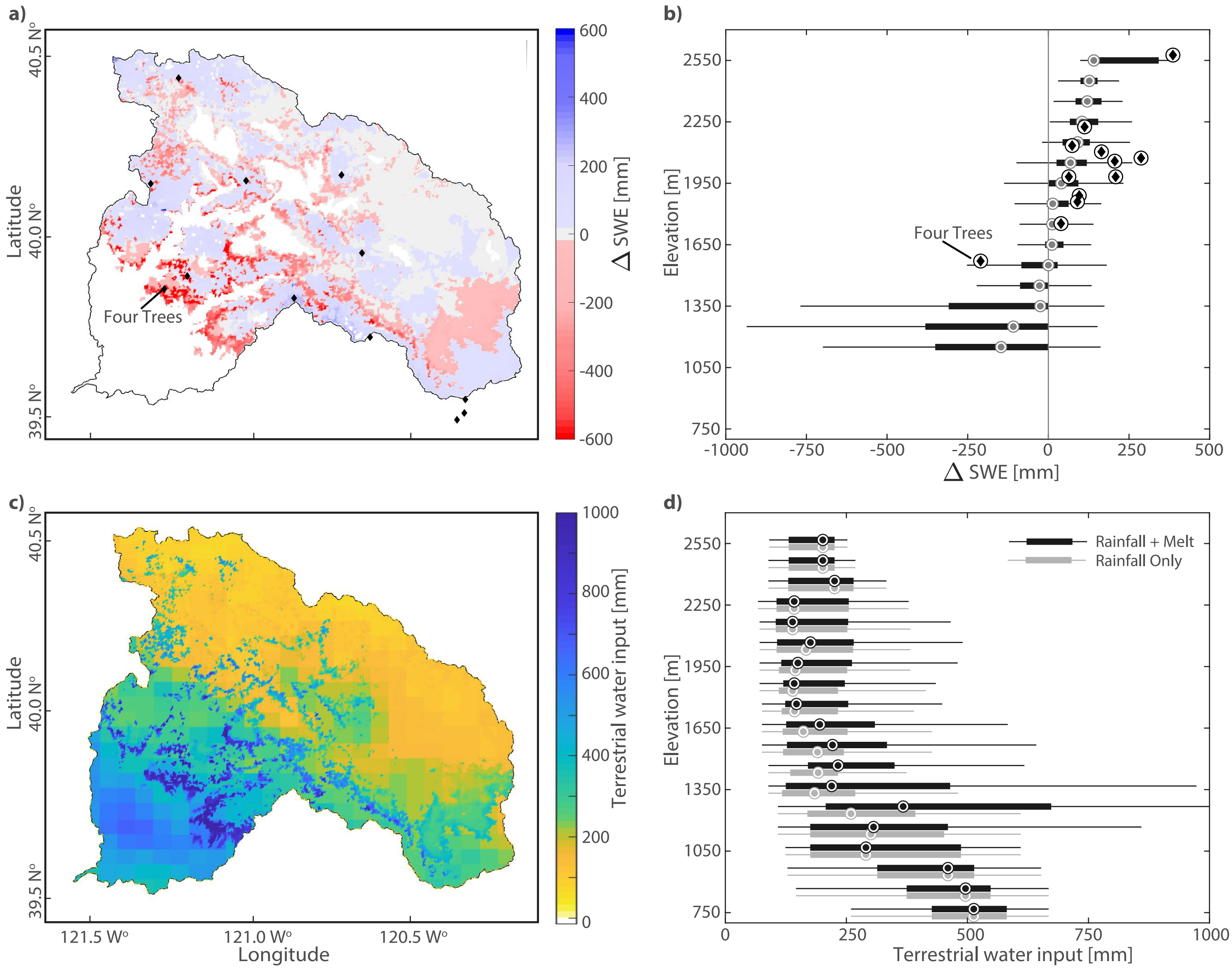

a)
b)
c)
d)
Four Trees
Four Trees
Latitude
Longitude
40.5 N°
40.0 N°
39.5 N°
121.5 W°
121.0 W°
120.5 W°
Δ SWE [mm]
600
400
200
0
-200
-400
-600
Elevation [m]
2550
2250
1950
1650
1350
1050
750
-1000
-750
-500
-250
0
250
500
Δ SWE [mm]
Terrestrial water input [mm]
1000
800
600
400
200
0
Rainfall + Melt
Rainfall Only
0
250
500
750
1000
Terrestrial water input [mm]